J. metamorphic Geol., 2004, **22,** 443–457 doi:10.1111/j.1525-1314.2004.00525.x

Trace element partitioning during high-*P* partial melting and melt-rock interaction; an example from northern Fiordland, New Zealand

F. C. SCHRÖTER[1], J. A. STEVENSON[1,*], N. R. DACZKO[1,2], G. L. CLARKE[1], N. J. PEARSON[2] AND K. A. KLEPEIS[3]
[1]*School of Geosciences, FO5, University of Sydney, Sydney, NSW 2006, Australia (geoffc@mail.usyd.edu.au)*
[2]*GEMOC ARC National Key Centre, Department of Earth and Planetary Sciences, Macquarie University, Sydney, NSW 2109, Australia*
[3]*Department of Geology, University of Vermont, Burlington, VT 05404, USA*

ABSTRACT Pods of granulite facies dioritic gneiss in the Pembroke Valley, Milford Sound, New Zealand, preserve peritectic garnet surrounded by trondhjemitic leucosome and vein networks, that are evidence of high-*P* partial melting. Garnet-bearing trondhjemitic veins extend into host gabbroic gneiss, where they are spatially linked with the recrystallization of comparatively low-*P* two-pyroxene-hornblende granulite to fine-grained high-*P* garnet granulite assemblages in garnet reaction zones. New data acquired using a Laser Ablation Inductively Coupled Plasma Mass Spectrometer (LA-ICPMS) for minerals in various textural settings indicate differences in the partitioning of trace elements in the transition of the two rock types to garnet granulite, mostly due to the presence or absence of clinozoisite. Garnet in the garnet reaction zone (gabbroic gneiss) has a distinct trace element pattern, inherited from reactant gabbroic gneiss hornblende. Peritectic garnet in the dioritic gneiss and garnet in trondhjemitic veins from the Pembroke Granulite have trace element patterns inherited from the melt-producing reaction in the dioritic gneiss. The distinct trace element patterns of garnet link the trondhjemitic veins geochemically to sites of partial melting in the dioritic gneiss.

Key words: garnet granulite; Laser Ablation Inductively Coupled Plasma Mass Spectrometer; partial melting; trace and REE; two-pyroxene hornblende granulite.

INTRODUCTION

Water-undersaturated partial melting of mafic lower continental crust is an important mechanism for the generation of intermediate and felsic magmas (e.g. Defant & Drummond, 1990; Atherton & Petford, 1993). Our understanding of this process in an inaccessible region is drawn indirectly from interpretations of experimental studies, rare exposures of lower crustal mafic to intermediate migmatites, and the geochemistry of mobilisates that have escaped their generation sites. Weaknesses in these interpretations include migmatitic textures commonly being ambiguous due to the effects of regional deformation and recrystallization, and our limited understanding of the abundance and distribution of many trace elements during partial melting (e.g. Bea *et al*., 1994).

Migmatitic textures are well exposed in dioritic gneiss of the Pembroke Granulite, northern Fiordland, New Zealand, which formed part of a Cretaceous lower crust (P = 12–14 kbar; T = 750–800 °C; Daczko *et al*., 2001a). Poikiloblastic garnet is surrounded by trondhjemitic leucosome in migmatitic textures, and the rocks experienced minimal strain during subsequent comparatively-rapid uplift (Daczko *et al*., 2001b). Melt escape from the Pembroke example is inferred to have been enhanced by fracture propagation and dyking through gabbroic gneiss, which encloses the pods of migmatitic dioritic gneiss. The migrating, water-deficient fluid (melt) is inferred to have scavenged water from the gabbroic gneiss and induced recrystallization in reaction zones that occur adjacent to the veins and dykes. These reaction zones in the gabbroic gneiss, hereafter referred to as garnet reaction zones (GRZ) (Blattner, 1976) – involved the near-isochemical replacement of a two-pyroxene hornblende assemblage by a garnet-clinopyroxene assemblage. In this paper, we present geochemical data obtained by an *in-situ* Laser Ablation Inductively Coupled Plasma Mass Spectrometer (LA-ICPMS) study of representative samples from these high-*P* migmatitic textures. The spatial resolution used by the LA-ICPMS provides an opportunity to examine the composition of individual minerals *in-situ*. The data are used to test previous interpretations of interaction

**Present address*: Department of Geology and Geophysics, Yale University, New Haven, CT 06520, USA.

between a migrating fluid (melt) and host rock in the GRZ, involving: (i) partial melting of dioritic gneiss; (ii) melt escape via fracturing and dyking; and (iii) interaction of migrating melt with gabbroic gneiss to form the array of GRZ (Daczko *et al.*, 2001a).

REGIONAL GEOLOGY AND PREVIOUS WORK

The study area is located in northern Fiordland in the Western Province of the South Island, New Zealand (Fig. 1), now dislocated by Late Tertiary movement along the Alpine Fault. The originally contiguous Westland-Nelson and Fiordland regions of the Western Province lie to the northwest and southeast of the fault, respectively. The study area lies within the Arthur River Complex, which encompasses the Pembroke Granulite and the Milford and Harrison Gneisses. Protoliths of these rocks include extensive Mesozoic magmatic-arc rocks, and Palaeozoic and Mesozoic screens and xenoliths (Tulloch *et al.*, 2000; Hollis *et al.*, 2003). Samples for this study were taken from the Pembroke Valley and an additional sample for comparison from Lake Pukutahi (5 km NE of the Pembroke Granulite; Fig. 1) within the Milford Gneiss. The Pembroke Granulite is a two-pyroxene, hornblende-bearing dioritic to gabbroic gneiss. It forms a low-strain zone within the homogeneous amphibolite to granulite facies metabasic Milford Gneiss (Blattner, 1976, 1991; Hill, 1995; Clarke *et al.*, 2000). The Harrison Gneiss is banded, comprising a dioritic host veined by abundant leucogabbroic and tonalitic layers (Blattner, 1991).

The Arthur River Complex experienced at least five deformation events at upper amphibolite to granulite facies conditions in the Early Cretaceous (Blattner, 1991; Clarke *et al.*, 2000; Daczko *et al.*, 2001a). The earliest structures are best preserved in the Pembroke Granulite, which includes gabbroic and dioritic gneiss, and contains a well-developed granulite facies foliation (S1) defined by two-pyroxene hornblende-bearing assemblages. In dioritic gneiss, S1 is cut by trondhjemitic leucosome that contains garnet poikiloblasts. In both dioritic and gabbroic gneiss, S1 is cut by steeply dipping planar fractures (D2) commonly filled by trondhjemitic veins with or without garnet. GRZ are developed adjacent to these trondhjemitic veins in the gabbroic gneiss but not in dioritic gneiss, even where a single vein cuts both units. A number of shear zones

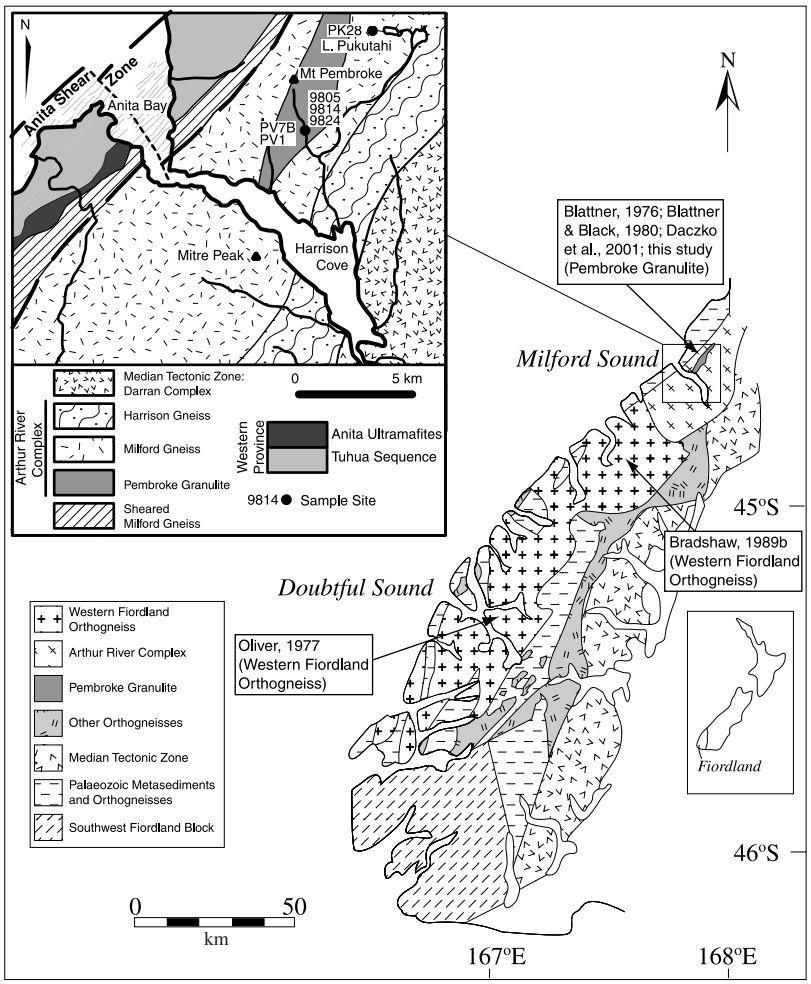

Fig. 1. Map of Fiordland, New Zealand, including the location of previous studies of garnet reaction zones (after Bradshaw, 1989). Blattner (1976); Blattner & Black (1980), and Daczko *et al.* (2001a,b) worked on samples taken from the Pembroke Granulite. Doubtful Sound was the field area of Oliver (1977). Bradshaw (1989) worked in the northern Western Fiordland Orthogneiss. Detailed map shows the geology of Milford Sound with sample locations in the Pembroke Granulite and at Lake Pukutahi in the Milford Gneiss.

and regional foliations cut S1 and GRZ; these are described elsewhere (Blattner, 1991; Clarke *et al.*, 2000; Daczko *et al.*, 2001a,b).

Garnet reaction zones developed adjacent to trondhjemitic veins have been described from localized areas across Fiordland (Fig. 1), and occur within a regionally-extensive Cretaceous batholith called the Western Fiordland Orthogneiss (Blattner, 1976; Oliver, 1977; Blattner & Black, 1980; Bradshaw, 1989; Daczko *et al.*, 2001a). Blattner (1976) first reported GRZ from the Pembroke Granulite and inferred that dehydration of the two-pyroxene-hornblende granulite (S1) assemblage was induced by flushing of CO_2-rich fluid phases along a pre-existing network of joints, later filled by trondhjemitic veins. Fracturing and garnet formation was inferred to have accompanied hornblende breakdown, through a decrease in the P/T ratio (Blattner & Black, 1980). Joint planes were inferred to have served as conduits for the transfer of mobile chemical constituents causing the differential loss of volatiles from the host gabbroic gneiss and controlling the metasomatic change to garnet granulite. Oliver (1977) inferred that GRZ in Doubtful Sound, some 100 km southwest of the Pembroke examples, formed from the partial melting of gabbroic gneiss. Melt was inferred to have migrated small distances to form trondhjemitic veins at the centre of a melt-depleted zone, the GRZ. As GRZ were only observed in the gabbroic gneiss in Doubtful Sound, Oliver (1977) inferred that this was the only unit that had experienced partial melting. Garnet reaction zones elsewhere in the Western Fiordland Orthogneiss were inferred by Bradshaw (1989) to have also formed by a metasomatic process. Again, carbonic fluids were inferred to have moved along a pre-existing network of joints and trondhjemitic veins and dehydrated the gabbroic gneiss host to form the GRZ. Minor changes in bulk rock composition and an increase in pressure were inferred to have played a part in the transition to garnet-granulite. Problems with the CO_2 flushing models include the nebulous source for carbonic fluids, an inability to account for the spatial interdependence of GRZ, fractures and trondhjemitic veins, and carbonate minerals being limited to comparatively rare scapolite (Blattner, 1991).

Daczko *et al.* (2001a) described widespread migmatitic textures in dioritic gneiss samples of the Pembroke Granulite. These authors inferred that partial melting, controlled by water-undersaturated hornblende breakdown in the dioritic gneiss, lead to a positive volume change that induced fracturing, assisting melt segregation and escape. Planar trondhjemitic veins are continuous across dioritic and gabbroic gneiss contacts. A water-poor melt is inferred to have escaped from the dioritic gneiss through fractures, where it invaded adjacent gabbroic gneiss that had not melted due to it having a higher temperature solidus. The melt is inferred to have scavenged water and dehydrated the host gabbroic gneiss, inducing a near isochemical change from hornblende-granulite to garnet-granulite. The spectacular rectilinear pattern of the fracture/vein/GRZ network is attributed to the late Cretaceous deviatoric stress field (Fig. 2a). Similar textures have been described in the Jijal complex of the Kohistan arc, Pakistan (Yamamoto & Yoshino, 1998).

FIELD RELATIONS AND PETROGRAPHY

Gabbroic gneiss is the most common rock in the Pembroke Granulite, forming more than 70% of exposures in the study area. Dioritic gneiss occurs in layers (tens of metres across) and discontinuous pods in the gabbroic gneiss. Ultramafic gneiss is less common, and mostly occurs as smaller pods in the other lithologies. Most rocks contain a gneissic foliation (S1) that envelops low-strain pods with coarse-grained, pyroxene-rich textures inherited from an igneous protolith. S1 is defined by pargasitic hornblende and plagioclase, with or without biotite, clinozoisite and quartz, reflecting conditions of $P < 8$ kbar and $T > 750$ °C (Clarke *et al.*, 2000). It strikes east to east-north-east and dips steeply towards the south and south-south-east. S1 is cut by a pattern of rectilinear fractures and trondhjemitic veins (D2). Bleached, pink, linear zones of garnet granulite occur parallel and adjacent to the veins and fractures in the network, and are known as GRZ (Fig. 2a). In gabbroic gneiss, the GRZ adjacent to the veins are up to a few centimetres wide. In dioritic gneiss they are either not observed or can only be recognized in thin section and are less than a millimetre wide. GRZ at Lake Pukutahi (Fig. 1) occur with similar structural patterns to those described above for gabbroic gneiss in the Pembroke Granulite, but only within metre-scale low-strain zones in the Milford Gneiss (Fig. 1). Most of the outcrops at Lake Pukutahi were extensively recrystallized during later deformation (D4); S1 and the GRZ are commonly deformed by narrow (< 1 m wide) dominantly sinistral mylonite zones and thrust faults (D3 & D4; Clarke *et al.*, 2000; Daczko *et al.*, 2002). Garnet granulite assemblages in the GRZ reflect conditions of $P \approx 14$ kbar and $T > 750$ °C (Clarke *et al.*, 2000). All samples used in this study were collected from outside D3 and D4 shear zones where the GRZ are best preserved.

Dioritic gneiss

Dioritic gneiss contains the S1 assemblage pargasitic hornblende, plagioclase, biotite, quartz and clinozoisite. S1 is cut by large (up to 25 mm across) garnet poikiloblasts that are enclosed by leucosome formed mostly from plagioclase and quartz (Fig. 2b; e.g. samples PV1, 9805). The leucosomes are interpreted by Daczko *et al.* (2001b) to represent sites of partial melting in the dioritic gneiss at > 750 °C. Where well developed, the garnet poikiloblasts may be aligned in

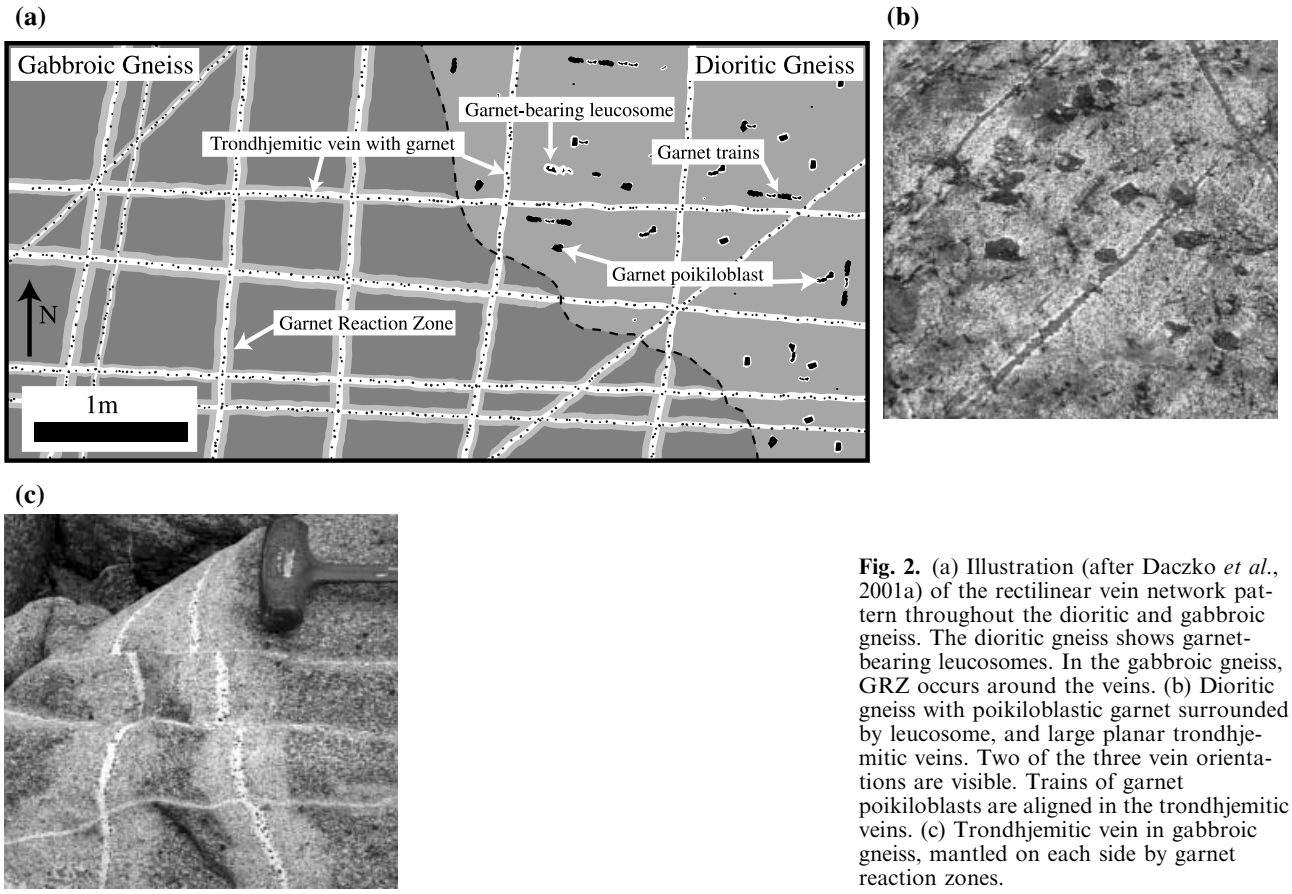

Fig. 2. (a) Illustration (after Daczko *et al.*, 2001a) of the rectilinear vein network pattern throughout the dioritic and gabbroic gneiss. The dioritic gneiss shows garnet-bearing leucosomes. In the gabbroic gneiss, GRZ occurs around the veins. (b) Dioritic gneiss with poikiloblastic garnet surrounded by leucosome, and large planar trondhjemitic veins. Two of the three vein orientations are visible. Trains of garnet poikiloblasts are aligned in the trondhjemitic veins. (c) Trondhjemitic vein in gabbroic gneiss, mantled on each side by garnet reaction zones.

trains that are enclosed by planar trondhjemitic veins (Fig. 2b) that display a planar lattice pattern comprising three vein sets: east-striking, north-striking, and north-east-striking (Clarke *et al.*, 2000, Fig. 4b; Daczko *et al.*, 2001a, Fig. 2c).

Two samples (9805, PV1) of well-foliated hornblende-plagioclase dioritic gneiss were analysed. Sample localities and representative electron microprobe and LA-ICPMS analyses of the minerals in each textural setting are presented in Table 1. Both of the dioritic gneiss samples contain hornblende-rich and plagioclase-rich domains, with biotite, quartz and clinozoisite common in the plagioclase-rich domains. Rutile, ilmenite and apatite occur in small proportions. Hornblende varies from idioblastic to sub-idioblastic, biotite is mostly idioblastic, and other grains are sub-idioblastic to xenoblastic. Large garnet poikiloblasts (up to 20 mm) occur, enclosed by leucosome of plagioclase and quartz, throughout the two samples analysed. Fine-grained symplectites (up to 1 mm across) of kyanite, plagioclase and quartz partially pseudomorph hornblende and plagioclase (dioritic gneiss) or plagioclase (leucosome) in sample PV1. The symplectites are inferred to have formed during high-P cooling of the terrane (Daczko *et al.*, 2002).

Gabbroic gneiss

The gabbroic gneiss contains a well-developed gneissic foliation (S1) defined by subhedral pargasitic hornblende, plagioclase and ilmenite, with or without orthopyroxene, clinopyroxene and quartz. Clusters of orthopyroxene and clinopyroxene with mutual exsolution blebs are preserved as large grains that are inferred to be relics from an igneous protolith. These igneous grains are mantled by S1 hornblende.

S1 is cut by trondhjemitic veins and fine-grained GRZ that partially recrystallized the dominant two-pyroxene-hornblende-plagioclase assemblages. Both define a lattice pattern matching that in the dioritic gneiss. The GRZ are usually symmetrical about trondhjemitic veins and of constant thickness (10–50 mm in width) in homogeneous gabbroic gneiss. Some trondhjemitic veins and related GRZ cut earlier veins and zones, suggesting that fracturing, veining, and garnet granulite formation were synchronous and episodic. GRZ in the gabbroic gneiss contain the assemblage garnet, clinopyroxene, rutile and plagioclase, with or without relict hornblende and orthopyroxene. Garnet and clinopyroxene intergrowths pseudomorph S1 hornblende and mimic

Table 1. Table showing sample locations and representative major (microprobe analyses) and trace element compositions (LA-ICPMS analyses) of minerals in each textural setting for samples taken from the Pembroke Granulite and Lake Pukutahi.

	Dioritic gneiss: 9805 (167°53′24.48″E 44°34′57.12″S); PV1 (167°53′24.13″E 44°34′57.0″S); PV7B (167°53′24.02″E 44°34′57.27″S)								
	Hbl (PV7B)	Plag (PV1)	Cz (PV1)	Bt (9805)	Ap (9805)	Ky (PV1)	Mus (9805)	Qtz (9805)	Rt (PV1)
SiO_2	41.33	63.19	38.51	35.61	0.12	36.78	46.69	99.54	0.04
TiO_2	1.04	0.01	0.09	1.41	0.00	0.00	0.88	0.03	97.55
Al_2O_3	14.78	23.63	27.34	18.79	0.02	62.01	33.16	0.00	0.00
Cr_2O_3	0.05	0.01	0.00	0.01	0.01	0.00	0.05	0.02	0.00
FeO	14.68	0.04	7.32	14.71	0.16	0.75	2.95	0.06	0.55
MnO	0.07	0.04	0.04	0.12	0.02	0.00	0.00	0.00	0.01
MgO	10.85	0.00	0.10	13.21	0.00	0.02	1.66	0.00	0.00
CaO	10.64	4.39	23.01	0.01	55.19	0.03	0.03	0.00	0.04
Na_2O	2.19	8.67	0.01	0.23	0.02	0.01	1.00	0.01	0.00
K_2O	1.09	0.08	0.01	8.30	0.00	0.00	8.89	0.00	0.00
Total	96.73	100.06	96.43	92.41	55.53	99.60	95.31	99.66	98.18
Li	12.8	1.5	0.24	147	0.3	97	21	0.04	0.57
Be	1.3	0.88	0.47	–	–	0.52	0.7	–	–
B	13	6.9	2.4	4.0	1.8	7.3	62	0.02	0.09
P	70	31	230	70	170000	25	53	4.9	6.3
Sc	45	1.5	43	13.1	0.59	6.4	8.6	0.02	0.07
V	490	0.02	240	810	1.06	159	550	–	11
Co	52	0.07	0.57	76	0.08	4	3.6	–	0.01
Ni	53	0.5	0.5	22	0.5	3.4	1.2	0.03	0.01
Cu	7	0.15	4.5	360	1.9	2.6	26	0.08	0.15
Ga	20	11	38	46	2.0	28	45	–	0.49
Rb	6.6	0.03	0.04	124	–	6.5	107	–	0.01
Sr	71	1490	3900	227	910	720	750	0.04	5.7
Y	3.5	0.01	42	2.2	94	1.9	0.20	0.00	0.002
Zr	19	–	9	3.4	5.4	1.1	1.05	–	1.2
Nb	0.056	–	–	0.08	0.03	0.01	0.07	–	0.6
Cs	0.048	0.31	–	20	–	0.84	5.4	–	–
Ba	221	58	50	10100	1.1	88	13500	–	0.30
La	0.056	0.00	43	0.20	0.49	1.6	–	–	–
Ce	0.33	–	87	0.38	2.2	3.9	–	–	–
Pr	0.070	–	12.4	0.05	0.47	0.52	–	0.00	–
Nd	0.46	–	57	0.4	3.1	5.7	–	–	–
Sm	0.18	–	13	0.16	1.7	0.79	0.13	–	–
Eu	0.14	0.01	6.8	0.53	1.4	0.45	0.07	–	–
Gd	0.33	–	12	–	5.0	0.44	–	–	–
Dy	0.59	–	9.2	–	10.8	0.26	–	–	–
Ho	0.13	–	1.7	0.05	3.2	0.06	–	–	–
Er	0.41	–	3.5	0.22	10.6	0.42	–	–	–
Yb	0.35	–	2.5	0.29	9.4	0.13	–	–	–
Lu	0.06	–	0.30	0.05	1.21	0.01	–	–	–
Hf	0.92	–	0.22	0.30	–	0.05	0.19	–	0.04
Pb	1.7	15.1	38	5.6	4.5	31	8.1	–	0.09
Th	–	–	0.88	–	20.6	0.24	–	–	–

	Gabbroic gneiss: 9814 (167°53′24.38″E 44°34′57.46″S); 9824 (167°53′24.47″E 44°34′57.51″S); PK28 (167°53′24.44″E 44°34′57.39″S)					
	Hbl (9814)	Plag (9824)	Opx (PK28)	Cpx (PK28)	Ap (9814)	Ky (9814)
SiO_2	40.80	57.48	51.34	52.08	0.11	37.31
TiO_2	1.57	0.00	0.03	0.16	0.04	0.00
Al_2O_3	15.22	26.22	3.36	3.38	0.00	62.81
Cr_2O_3	0.03	0.01	0.03	0.06	0.00	0.00
FeO	15.42	0.00	22.99	8.47	0.32	1.27
MnO	0.21	0.01	0.76	0.34	0.12	0.00
MgO	9.71	0.00	20.57	12.53	0.00	0.00
CaO	10.77	8.76	0.48	20.97	54.35	0.05
Na_2O	2.59	7.03	0.02	1.56	0.04	0.00
K_2O	0.66	0.16	0.02	0.00	0.00	0.01
Total	96.97	99.67	99.59	99.55	54.98	101.45
Li	7.7	0.77	7.3	8.7	22	3.7
Be	1.3	–	–	0.33	–	–
B	3.1	2.7	4.0	2.8	20	4.5
P	86	91	130	80	52000	130
Sc	45	0.27	21.1	126	122	1.5
V	460	–	207	275	1440	66
Co	57	–	96	32	183	0.52
Ni	30	–	44	24	98	1.4
Cu	23	2.0	99	76	280	114
Ga	23	18	17.5	7.4	83	53
Rb	3.3	–	0.05	0.06	10.1	0.4
Sr	124	1720	2.8	47	650	1000

Table 1. (*Cont'd*).

	Gabbroic gneiss: 9814 (167°53′24.38″E 44°34′57.46″S); 9824 (167°53′24.47″E 44°34′57.51″S); PK28 (167°53′24.44″E 44°34′57.39″S)					
	Hbl (9814)	Plag (9824)	Opx (PK28)	Cpx (PK28)	Ap (9814)	Ky (9814)
Y	18	0.07	0.9	11	152	3.2
Zr	19	–	2.9	30	47	2.1
Nb	1.17	–	–	0.10	2.7	–
Cs	0.05	–	0.11	0.05	0.2	–
Ba	123	328	2.6	18.7	430	12.3
La	0.27	4.5	0.60	1.3	67	12.0
Ce	3.8	5.4	0.54	6.9	290	20.5
Pr	1.57	0.47	0.08	1.6	57	2.2
Nd	12.6	1.1	0.46	8.3	270	8.4
Sm	4.5	0.15	0.10	2.6	59	0.9
Eu	1.7	0.17	0.04	0.76	18.4	1.9
Gd	4.5	–	0.13	2.6	49	0.7
Dy	3.7	–	0.12	2.4	31	–
Ho	0.70	–	–	0.46	6.2	–
Er	1.8	–	0.09	1.1	14.5	0.6
Yb	1.4	–	0.11	1.04	9.0	–
Lu	0.20	–	0.02	0.15	1.4	–
Hf	0.69	–	0.07	1.22	1.2	–
Pb	1.1	9.6	0.12	0.51	6.8	6.3
Th	–	–	0.05	0.07	2.6	–

	Garnet reaction zone: 9814 (167°53′24.38″E 44°34′57.46″S); 9824 (167°53′24.47″E 44°34′57.51″S); PK28 (167°53′24.44″E 44°34′57.39″S)					
	Grt (9814)	Plag (PK28)	Cz (9814)	Cpx (9824)	Ap (9824)	Ill (PK28)
SiO_2	39.11	57.30	38.50	52.06	0.10	0.00
TiO_2	0.04	0.00	0.08	0.27	0.02	27.05
Al_2O_3	21.92	27.40	27.22	4.86	0.00	0.00
Cr_2O_3	0.01	0.01	0.06	0.04	0.00	0.30
FeO	22.72	0.00	8.29	8.01	0.03	65.72
MnO	0.46	0.00	0.06	0.14	0.01	0.00
MgO	9.37	0.00	0.09	11.39	0.00	0.33
CaO	6.55	8.91	22.85	19.60	55.00	0.00
Na_2O	0.02	6.27	0.03	2.65	0.08	0.02
K_2O	0.01	0.14	0.00	0.01	0.00	0.00
Total	100.20	100.03	97.18	99.02	55.24	93.42
Li	4.7	1.2	–	38	3.3	1.23
Be	0.06	0.87	–	1.8	0.47	–
B	1.3	7.7	1.7	5.9	4.6	0.6
P	210	42	145	12.7	93000	19
Sc	60	0.91	2.7	132	3.3	6
V	240	0.08	15	370	14	5500
Co	65	0.05	0.78	33	8.8	37
Ni	7.6	0.60	0.44	31	20	32
Cu	6.9	0.12	18	8.4	12	6.9
Ga	18	18	47	19	41	10.5
Rb	0.21	0.02	–	0.02	0.93	0.36
Sr	5.3	1800	3000	72	1710	1.16
Y	30	0.04	3.6	6.5	206	0.117
Zr	4.0	0.01	8	58	7.0	4.5
Nb	0.41	–	–	0.04	0.10	4.0
Cs	0.01	–	–	0.01	–	–
Ba	1.5	170	41	1.9	107	0.57
La	0.23	2.0	33	3.4	560	0.023
Ce	1.1	2.6	53	14	1360	0.27
Pr	0.25	0.19	5.5	2.9	179	0.018
Nd	2.1	0.60	17	16	710	0.053
Sm	2.6	0.05	2.0	4.1	111	0.017
Eu	1.3	0.15	2.9	1.3	38	0.019
Gd	4.9	0.02	1.2	2.9	80	0.017
Dy	5.6	–	0.54	1.8	44	–
Ho	1.08	–	0.08	0.26	7.8	0.003
Er	2.9	–	0.23	0.57	18.8	–
Yb	2.3	–	0.26	0.39	11.8	–
Lu	0.31	–	–	0.06	1.71	–
Hf	0.13	0.01	–	2.3	0.16	0.21
Pb	0.18	8.9	20	0.56	15	0.156
Th	0.02	–	0.30	0.30	32	0.008

Table 1. (*Cont'd*).

	Leucosome: 9805 (167°53′24.48″E 44°34′57.12″S); PV1 (167°53′24.13″E 44°34′57.0″S)						
	Plag (9805)	Cz (PV1)	Grt (PV1)	Ap (PV1)	Mus (PV1)	Qtz (PV1)	Rt (PV1)
SiO_2	63.77	38.53	38.59	0.02	47.41	100.07	0.00
TiO_2	0.00	0.15	0.07	0.00	0.65	0.00	97.44
Al_2O_3	22.32	26.67	21.49	0.00	33.60	0.00	0.00
Cr_2O_3	0.00	0.05	0.00	0.04	0.07	0.01	0.00
FeO	0.01	7.93	25.34	0.01	3.26	0.06	0.56
MnO	0.02	0.19	1.84	0.00	0.03	0.00	0.03
MgO	0.00	0.07	5.32	0.00	1.64	0.00	0.00
CaO	3.68	23.19	7.79	56.07	0.00	0.05	0.02
Na_2O	9.66	0.02	0.02	0.05	1.12	0.01	0.00
K_2O	0.12	0.03	0.00	0.00	9.10	0.00	0.00
Total	99.59	96.82	100.46	56.19	96.89	100.20	98.05
Li	0.78	0.10	6.9	0.88	22	0.03	0.013
Be	0.52	0.19	–	–	0.32	–	–
B	75	1.2	1.8	0.7	40	0.05	–
P	17	200	50	130000	100	14	3.3
Sc	1.2	36	30	0.37	10.4	0.01	0.19
V	–	240	80	14.0	380	0.01	21
Co	0.16	0.6	42	2.3	3.3	0.00	0.17
Ni	0.39	0.34	0.67	1.8	1.6	0.01	–
Cu	0.0001	0.4	6.0	3.5	3	0.01	0.6
Ga	8	42	5.5	3.0	31	0.01	0.016
Rb	–	–	0.28	0.10	90	0.16	–
Sr	1100	3700	3.1	550	700	0.31	0.05
Y	0.03	41	15.5	36	0.27	0.02	0.092
Zr	–	7	6.5	0.15	0.89	0.81	3.8
Nb	–	–	0.05	–	0.06	0.00	2.1
Cs	–	–	0.05	–	7	0.00	–
Ba	96	23	6.1	2.6	8500	1.45	0.016
La	0.02	44	–	3.1	0.061	0.02	–
Ce	0.02	93	0.01	9.4	0.14	0.05	–
Pr	–	13	–	1.6	0.019	0.01	–
Nd	–	58	–	10	0.10	0.02	–
Sm	–	12	0.04	3.1	0.06	0.00	–
Eu	–	6.7	0.04	1.3	0.038	0.00	0.0010
Gd	–	11	0.34	4.1	–	0.00	0.004
Dy	–	9	1.6	5.4	–	0.00	0.009
Ho	–	1.6	0.55	1.3	–	0.00	0.0027
Er	–	3.8	2.0	4.3	–	0.00	0.015
Yb	–	2.9	3.4	4.3	–	0.00	0.032
Lu	–	0.35	0.63	0.61	–	0.00	0.0059
Hf	–	0.27	0.07	–	0.09	0.02	0.12
Pb	4.5	40	0.70	1.0	9	0.04	0.003
Th	–	1.8	–	–	–	0.01	–

	Trondhjemitic vein: 9814 (167°53′24.38″E 44°34′57.46″S); PK28 (167°53′24.44″E 44°34′57.39″S); PV7B (167°53′24.02″E 44°34′57.27″S)					
	Grt (9814)	Grt (PK28)	Plag (PV7B)	Plag (PK28)	Qtz (PK28)	Ap (9814)
SiO_2	38.27	39.31	64.03	57.72	99.82	0.01
TiO_2	0.16	0.06	0.00	0.00	0.00	0.00
Al_2O_3	21.17	21.68	23.03	26.98	0.01	0.00
Cr_2O_3	0.00	0.01	0.00	0.00	0.02	0.07
FeO	25.39	22.13	0.01	0.00	0.03	0.07
MnO	1.64	0.24	0.03	0.06	0.00	0.05
MgO	7.59	8.44	0.00	0.00	0.00	0.00
CaO	5.94	7.91	3.98	8.45	0.02	54.94
Na_2O	0.04	0.01	9.18	6.49	0.00	0.12
K_2O	0.00	0.01	0.13	0.22	0.00	0.00
Total	100.20	99.79	100.40	99.92	99.89	55.26
Li	5.2	4.1	0.33	0.95	0.02	1.29
Be	–	–	0.35	0.72	0.0006	–
B	0.81	3.2	11	11	0.03	1.2
P	100	130	22	47	0.17	180000
Sc	64	40	1.4	1.3	0.012	0.09
V	140	410	0.01	0.39	0.008	1.69
Co	44	60	0.91	0.23	0.001	0.16
Ni	1.8	19	1.6	4.2	0.01	0.48
Cu	3.4	50	1.3	360	0.01	34
Ga	9.2	28	11	20	0.01	9.0
Rb	0.02	0.11	0.19	2.5	0.12	0.06
Sr	0.06	6.3	1250	2270	0.15	1370
Y	110	15	0.07	0.09	0.02	83
Zr	30	7	0.01	0.01	0.54	3.6

Table 1. (*Cont'd*).

	Trondhjemitic vein: 9814 (167°53′24.38″E 44°34′57.46″S); PK28 (167°53′24.44″E 44°34′57.39″S); PV7B (167°53′24.02″E 44°34′57.27″S)					
	Grt (9814)	Grt (PK28)	Plag (PV7B)	Plag (PK28)	Qtz (PK28)	Ap (9814)
Nb	–	–	–	0.01	0.004	–
Cs	–	0.7	0.01	0.12	0.002	–
Ba	0.02	0.9	240	200	0.74	2.0
La	0.01	0.14	0.01	1.6	0.02	249
Ce	0.04	1.5	0.02	2.5	0.03	680
Pr	0.04	0.30	0.01	0.25	0.004	95
Nd	0.84	2.8	–	0.96	0.02	400
Sm	1.63	2.3	–	0.08	0.004	69
Eu	1.07	1.03	0.01	0.13	0.001	17.8
Gd	6.4	2.8	–	0.02	0.003	47
Dy	16	2.8	–	–	0.003	21.0
Ho	4.12	0.56	–	–	0.0006	3.1
Er	13	1.3	–	–	0.002	5.2
Yb	14	1.2	–	–	0.002	2.2
Lu	2.2	0.18	–	–	0.0003	0.23
Hf	0.38	0.10	–	0.01	0.02	–
Pb	2.0	0.26	12.8	9.6	0.03	4.2
Th	–	2.5	–	–	0.01	8.5

the S1 gneissic foliation. Samples of gabbroic gneiss analysed via LA-ICPMS include host gneiss (9814, 9824, PK28), GRZ (9814, 9824, PK28) and trondhjemitic veins (9814, 9824, PK28). The vein samples from dioritic and gabbroic hosts are described in detail below.

Veins

The trondhjemitic veins are commonly less than 5 mm in width, although examples up to 30 mm wide occur. They are dominantly (*c*. 90%) oligoclase with less garnet, kyanite, quartz, clinozoisite and hornblende, and rare clinopyroxene and scapolite. Scapolite is most common in larger pegmatitic veins (up to 10 cm wide) where a euhedral form and concentric chemical zoning are consistent with an igneous origin. Veins in the dioritic gneiss are spatially linked to garnet poikiloblasts and occur as one of three types: (1) thick veins (>10 mm) with trains of large garnet grains at their centres (Fig. 2b); (2) very thin veins (<5 mm) that have garnet poikiloblasts/leucosomes a few centimetres on either side of the vein in the host rock; and (3) veins with trains of garnet grains at their edges (Daczko *et al.*, 2001b), either symmetrical disposed on both vein walls or asymmetrically developed on a single side. In the gabbroic gneiss the veins are mantled by GRZ, and commonly have trains of garnet grains along one or both edges, similar to leucosome textures in the dioritic gneiss (Fig. 2c). Across the contact between dioritic and gabbroic gneiss trondhjemitic veins change from being garnet-bearing in dioritic gneiss to being comparatively garnet-poor in gabbroic gneiss (Fig. 2c, Daczko *et al.*, 2001b). Vein-gneiss contacts are sometimes sharply defined but also commonly exhibit interlocking grains consistent with fracture healing.

Four vein samples were analysed via electron microprobe and LA-ICPMS. Sample PV7B was taken from a dioritic gneiss cut by a trondhjemitic vein (Fig. 3a). The vein contains a train of small (<3 mm) garnet grains along the host dioritic gneiss contact. Texturally, this sample can be divided into two areas:

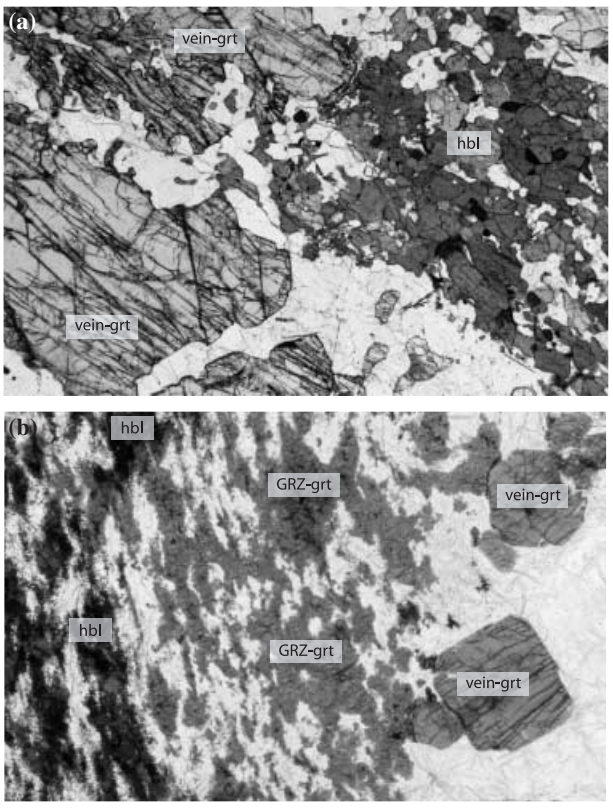

Fig. 3. (a) Photomicrograph (sample PV7B; base: 5.2 mm) of a dioritic gneiss – trondhjemitic vein transition. The right side of picture shows hornblende dominated host rock (dioritic gneiss). The left side of the picture shows garnet in trondhjemitic vein. Light areas are predominantly plagioclase with quartz. (b) Flatbed scan of a 100 μm thin section (sample 9814; base: 3.5 cm). Scan displays three textural settings: hornblende dominated gabbroic gneiss on the left side, GRZ in the centre and trondhjemitic vein on the right side.

(1) well-foliated hornblende-plagioclase dioritic gneiss, similar to samples 9805 and PV1; and (2) plagioclase-rich trondhjemitic vein. Large idioblastic garnet (up to 5 mm across), with rare inclusions of quartz and rutile, occur at the margin of the vein.

Three samples (9814, 9824 both Pembroke Granulite; PK28 from Lake Pukutahi) were taken from gabbroic gneiss cut by trondhjemitic veins. The veins have euhedral garnet studded along their margins and well-developed GRZ adjacent to the vein margins (Fig. 3b). These gabbroic gneiss samples may be further sub-divided into three domains. The first domain represents S1 assemblage where the hornblende-plagioclase gabbroic gneiss has a granoblastic texture. The second domain includes the GRZ where large grains of garnet (up to 3 mm across) are intergrown with fine-grained clinopyroxene in a plagioclase matrix. Garnet contains numerous inclusions, mostly of quartz and less rutile. Garnet is idioblastic where in contact with plagioclase. Orthopyroxene is rare and mantled by garnet granulite assemblages.

Relict pyroxene is generally sub-idioblastic. The third domain is the trondhjemitic vein with or without inclusion-poor euhedral garnet (up to 12 mm across) along the vein margin. These veins also contain rare kyanite and clinopyroxene grains (up to 4 mm across) along the boundary of the vein and the GRZ. Clinopyroxene occurs intergrown with, and as inclusions in, garnet in the trondhjemitic veins.

Mineral chemistry

Analyses for mineral chemistry were performed on the Cameca SX50 Electron Microprobe (EM Unit, University of New South Wales, Sydney Australia) for major elements and on the Merchantek EO LUV laser-ablation microprobe attached to a Nu Plasma multi-collector ICPMS, at Macquarie University for trace elements. The Merchantek LUV laser system delivers a beam of 266 nm UV light from a frequency-coupled Nd:YAG laser. The laser drilled cylindrical flat-bottomed pits of 30 μm diameter. The spatial resolution and excellent optical-viewing system of the laser microprobe allowed high resolution positioning of each analysis. The external standard was the NIST610 glass standard; Ca was used as the internal standard for garnet, clinopyroxene, plagioclase, hornblende, clinozoisite, apatite, quartz and rutile; Al was used for orthopyroxene, kyanite, muscovite and biotite. A NIST612 glass standard and a BCR 2 standard were used to confirm that the analyses were accurate. Data were processed online using the GLITTER software (http://www.mq.edu.au/GEMOC/) for processing time-resolved signals. Hardware, operating conditions, and methods are otherwise as described by Norman *et al.* (1996, 1998). The results of mineral analyses have all been normalized to chondrite values used in the Glitter software (Taylor & McLennan, 1985). The following mineral compositional descriptions refer to these normalized values unless otherwise stated (i.e. enriched or depleted, relative to chondrite).

The mineral analyses are divided into five textural settings:
(1) gabbroic gneiss, including relict igneous textures;
(2) dioritic gneiss;
(3) leucosome as part of migmatitic textures in the dioritic gneiss;
(4) trondhjemitic veins that are continuous across the contact of dioritic and gabbroic gneiss; and
(5) garnet reaction zones (GRZ).

Table 1 includes a list of analysed elements and characteristic analyses for each mineral type from the various textural settings. In the following description, we outline the main characteristics of each mineral group from the different textural settings.

Garnet occurs in textural settings 3, 4 and 5. Major-element and trace-element compositions distinguish garnet from each of these settings (Fig. 4a–c). Garnet in migmatitic textures within the dioritic gneiss (setting 3) displays a REE pattern that shows depletion in LREE and enrichment in HREE. LREE contents are frequently below detection limits. Garnet in trondhjemitic veins (setting 4) from the two sample sites (Pembroke and Pukutahi) is distinct in terms of trace element patterns, but consistent within each site. Garnet in trondhjemitic veins from the Pembroke Granulite (i) shows a trend of increasing enrichment from Nd to Lu; garnet from Lake Pukautahi (ii) shows an increasing trend of enrichment from Nd to Eu and a decreasing trend of enrichment from Gd to Lu (Fig. 4b). In GRZ (setting 5) garnet shows a similar pattern of decreasing HREE to group (ii) garnet in the trondhjemitic veins, although LREE values are generally slightly higher. Hf values in all three settings are scattered at normalized values close to one.

Hornblende in gabbroic (setting 1) and dioritic (setting 2) gneiss has distinct trace element patterns (Fig. 4d,e). Hornblende in gabbroic gneiss is enriched in Ti, Y and HREE when compared with hornblende from dioritic gneiss. Rb, Nb and LREE are commonly enriched in hornblende from gabbroic gneiss and depleted in hornblende from dioritic gneiss. Conversely, hornblende from the dioritic gneiss generally has higher normalized values of Li, B, and, to a less extent, Pb. Th was close to detection limits in hornblende from the dioritic gneiss and was not detected in hornblende from gabbroic gneiss.

Clinopyroxene is commonly observed as relict igneous grains in the gabbroic gneiss, and as metamorphic grains in GRZ (settings 1 & 5; Fig. 4f). Clinopyroxene in both settings generally has identical major and trace element patterns, including the REE. Subtle differences involve lower normalized values of Mn, Y, Cs and HREE, and higher values of Be, V and Ga, for clinopyroxene from the GRZ (setting 5). The ranges in REE distribution from clinopyroxene in both textural settings overlap.

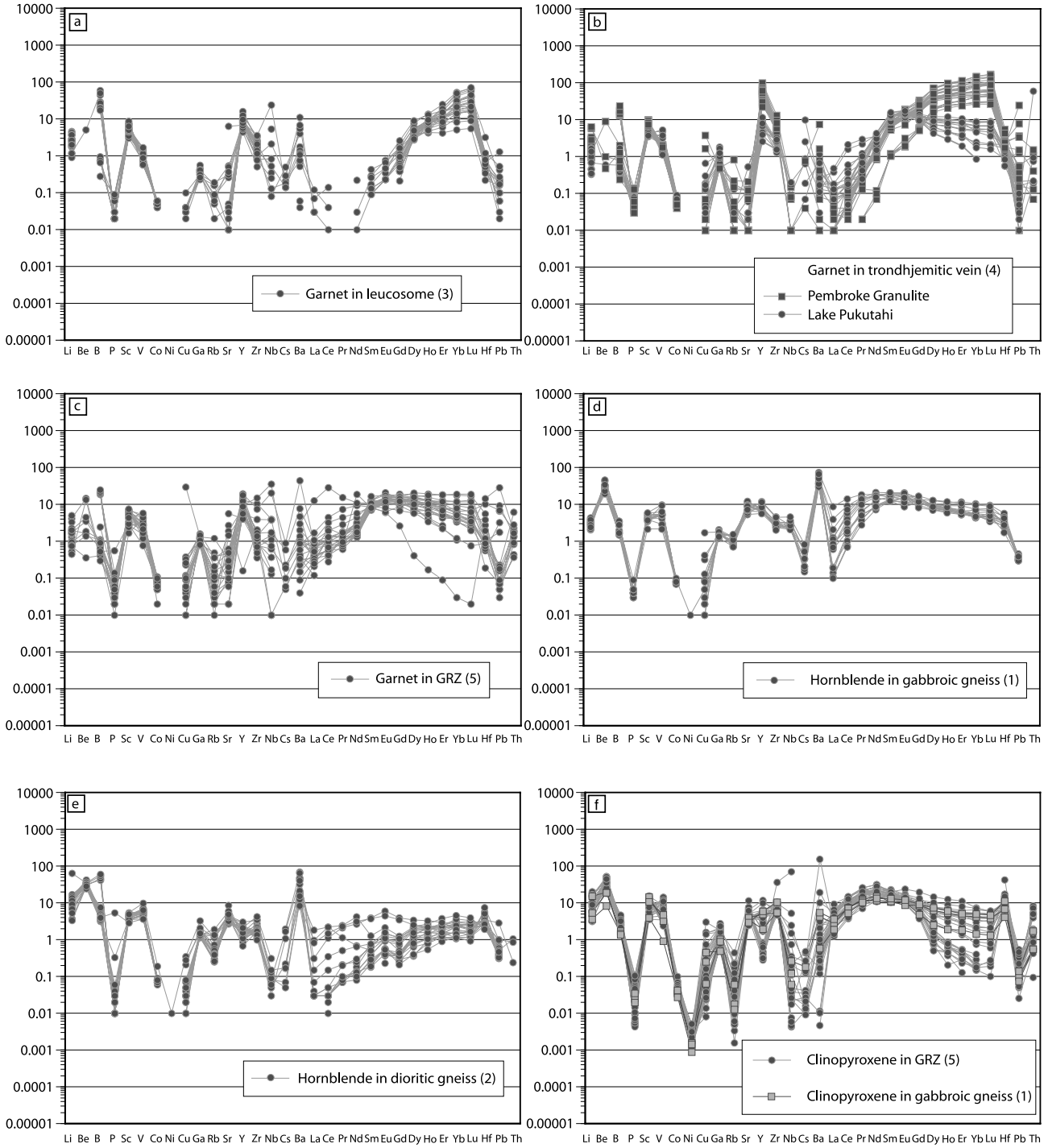

Fig. 4. Plots of trace element normalized to chondrite of critical minerals from different settings: (a) garnet from leucosomes in dioritic gneiss (setting 3); (b) garnet from trondhjemitic veins (setting 4); (c) garnet from GRZ (setting 5); (d) hornblende from gabbroic gneiss (setting 1); (e) hornblende from dioritic gneiss (setting 2); (f) clinopyroxene from GRZ (setting 5) and gabbroic gneiss (setting 1); (g) orthopyroxene from gabbroic gneiss (setting 1); (h) clinozoisite from dioritic gneiss (setting 2), leucosomes (setting 3) and GRZ (setting 5); (i) biotite from dioritic gneiss (setting 2); (j) plagioclase from dioritic gneiss (setting 2) and leucosomes (setting 3); (k) plagioclase from gabbroic gneiss (setting 1) and GRZ (setting 5); (l) plagioclase from trondhjemitic veins (setting 4).

Orthopyroxene (Fig. 4g) is observed as relict igneous grains, both in the gabbroic gneiss (setting 1) and in the GRZ (setting 5). It has no significant enrichment in any of the measured elements, except for Li, B, Sc and V. All other normalized trace element concentrations indicate depletion.

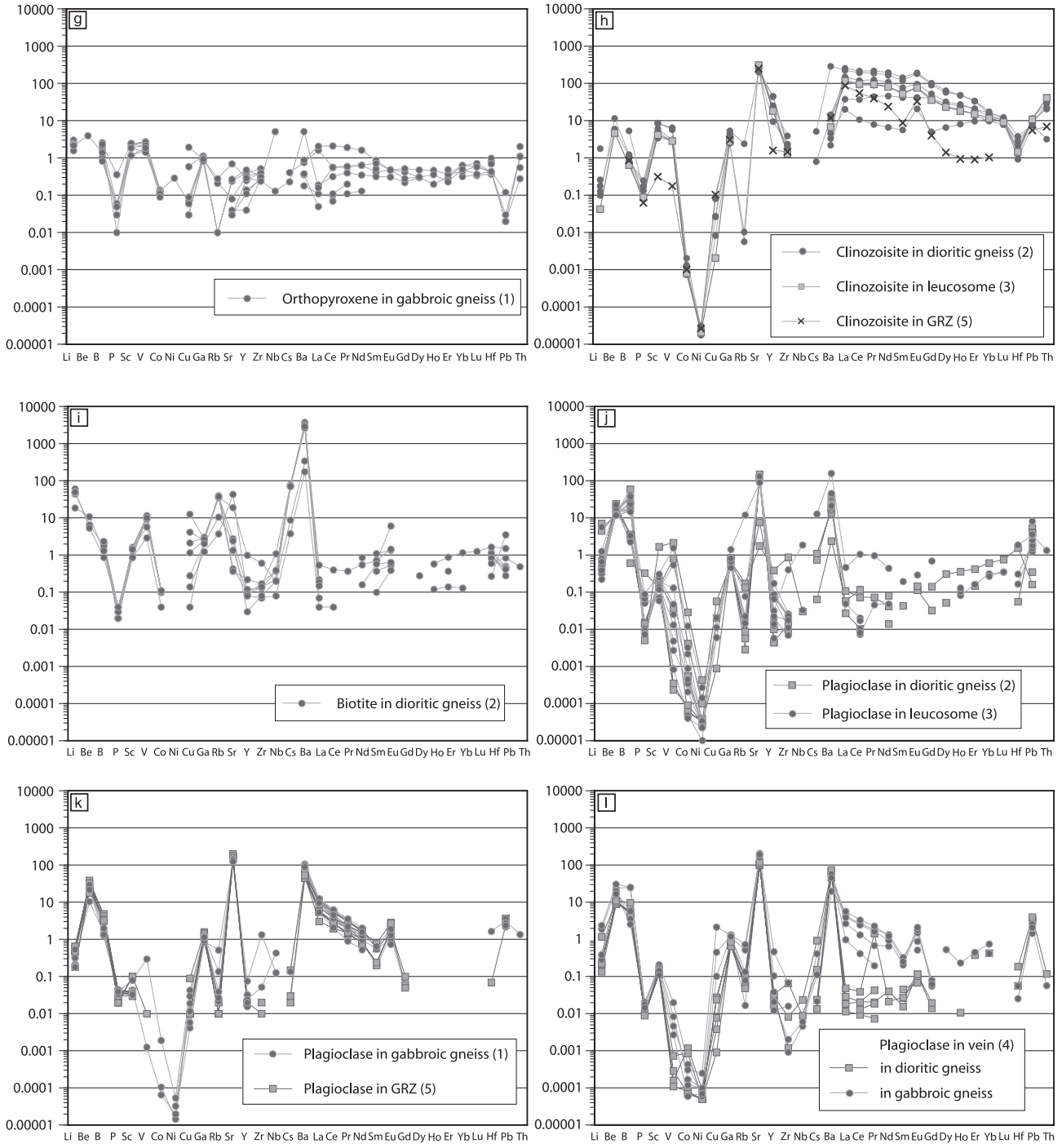

Fig. 4. (*Cont'd*).

Clinozoisite is of small grain size, and so only a few analyses could be carried out in dioritic gneiss (setting 2), in migmatitic textures (setting 3) and in the GRZ (setting 5; Fig. 4h). Clinozoisite displays enrichment in the trace elements Be, Sc, V, Ga, Zr, Ba, Hf and Pb as well as pronounced enrichment in Sr, Y, Th and REE. The REE generally display a decreasing trend of enrichment with a weak positive Eu anomaly. Clinozoisite from the GRZ is the exception to this pattern; it shows depletion in Sc and V and a lesser enrichment in Y, Th and the HREE.

Biotite is common in small proportions in the dioritic gneiss (setting 2, Fig. 4i). Normalized values of Li, Be, B, Sc, V, Ga, Rb and Cs indicate slight to moderate

enrichment. Ba is strongly enriched and forms a prominent positive peak. Cu, Sr and Pb concentrations scatter near a ratio of one. The LREE are subtly depleted. The HREE display a trend from being slightly depleted to slightly enriched as the atomic number is increased.

Plagioclase has similar trace-element patterns (excluding REE) in all the analysed textural settings (Fig. 4j–l). Almost all plagioclase analyses show distinct Be, B, Sr and Ba enrichment spikes. On the basis of REE composition, two patterns can be distinguished. Plagioclase in dioritic gneiss (setting 2) and leucosome (setting 3) has REE concentrations that are depleted and subtly scattered, but show a general increasing trend in Lu, almost reaching a ratio of one. Hf scatters at normalized values close to one. In the gabbroic gneiss (setting 1) and the GRZ (setting 5), plagioclase has a distinct REE pattern involving a decreasing trend of enrichment in the LREE towards Sm, which is slightly depleted. Eu values define a small but characteristic positive anomaly. With the exception of Gd, which follows the decreasing trend, none of the HREE concentrations could be detected. Hf in settings 1 and 5 is rarely above detection limits, but where data could be obtained values were similar to those from settings 2 and 3. Trace and REE-patterns found in plagioclase from trondhjemitic veins (setting 4) repeat the characteristic trend of settings 2 and 3 (when cutting dioritic gneiss) as well as settings 1 and 5 (when cutting gabbroic gneiss).

Rutile is observed in most textural settings, but due to grain size constraints it could only be analysed in samples of the dioritic gneiss (setting 2), in leucosomes (setting 3) and in the GRZ (setting 5). Calcium was used to calibrate rutile analyses, but is only present in small concentrations; the accuracy of these analyses may be questionable, although general trends should remain unchanged. Rutile analyses from all settings are generally depleted (1/10 to 1/1000) in trace and REE with rare exceptions being V, Zr, Hf (only slightly depleted) and Nb (slightly enriched). Due to the quantity of analysed grains and the number of values below detection limits rutile from the different settings could not be compared satisfactorily.

Quartz in the dioritic gneiss (setting 2), leucosomes (setting 3) and trondhjemitic veins (setting 4) is depleted in all trace elements. The precision of these analyses is questionable due to the internal calibration with Ca and its low concentration in quartz. A number of element concentrations were below detection limits, especially for the MREE and HREE, resulting in a disjointed element pattern. Quartz from the trondhjemitic vein (setting 4) displays a complete element pattern that decreases from LREE towards elements of higher atomic numbers. Concentrations of the HREE are constant and very low.

Kyanite was analysed in gabbroic (setting 1) and dioritic gneiss (setting 2). Again, due to grain size constraints there are few analyses. Kyanite from both settings shows the same general pattern, but with irregular variations. Normalized values of the trace elements Li, Be, B, Ga, Sr and Ba show a slight to moderate enrichment. V, Pb, Th, LREE and MREE concentrations scatter at normalized values close to one, with a general trend of enrichment especially in the LREE. The REE concentrations generally show a trend of decreasing enrichment towards higher atomic numbers, with a weak to moderate positive Eu peak. In general, the HREE are slightly depleted. In one case all REE were below detection limits.

Muscovite (phengitic white mica) in the dioritic gneiss (setting 2) has trace element concentrations characterized by enrichment peaks in Li, Be, B, V, Ga, Rb, Sr, Cs, Pb and a major spike in normalized Ba content. The REE were rarely present above detection limits, with the exception of Sm and Eu, which are scattered at normalized values close to one. Sc and Hf also have normalized values close to one.

Apatite analyses were collected for all five textural settings, but with limited analyses in the dioritic gneiss (setting 2) due to grain size constraints. Apatite from the dioritic gneiss (setting 2) shows enrichment in Sr, Y, REE and Th. The REE contents show a weak enrichment trend for elements with higher atomic number, with a slight decrease in Yb and Lu. Be, Cs and Hf concentrations were below detection limits. Apatite from leucosomes in the dioritic gneiss (setting 3) displays the same general pattern with the exception of Th, which was not detected. Apatite from the trondhjemitic vein (setting 4) has a similar pattern to apatite in the dioritic gneiss (setting 2), but is strongly enriched in the LREE with a trend of decreasing enrichment for elements with higher atomic number. HREE contents of apatite in the vein show the same pattern of enrichment as apatite in the dioritic gneiss (setting 3). Apatite from the gabbroic gneiss (setting 1) has some distinctions; it is enriched in B, Sc, V, Cu, Ga, Rb, Zr, Nb, Ba and Hf. In one of two analyses, apatite in the gabbroic gneiss is comparatively enriched in Be and Cs with normalized values close to one. The REE patterns for apatite in the gabbroic gneiss have two distinct trends. One is much the same as for apatite in the dioritic gneiss, and the second involves more strongly enriched LREE and a pattern of increasing enrichment of the elements between La and Pr/Nd, followed by a decreasing pattern, but still with enriched values, from there to the HREE. The trace elements from apatite in the GRZ (setting 5) plot in-between the values from the gabbroic gneiss and the dioritic gneiss. The REE pattern of apatite in the GRZ is slightly enriched, but basically similar to apatite from the trondhjemitic vein.

Ilmenite was analysed in the GRZ (setting 5) and displays weak to moderate enrichment in V, Nb and Hf. LREE contents are slightly depleted with a decreasing trend towards MREE. HREE contents are below detection limits.

DISCUSSION

Origin of the trondhjemitic veins

Previous work has related the trondhjemitic veins in the gabbroic gneiss to sites of partial melting in the dioritic gneiss, on the basis of field criteria and textural evidence (Daczko *et al*., 2001a). Preliminary piston-cylinder experiment data (Antignano *et al*., 2001) suggests that incongruent melting of the dioritic gneiss assemblage involved the reaction:

$$\text{hornblende} + \text{plagioclase1} + \text{quartz} \pm \text{biotite} \pm \text{clinozoisite} \rightarrow \text{garnet} + \text{plagioclase2} + \text{melt} \quad (1)$$

Considering the reactants in reaction 1, it is likely that biotite controlled the earliest melting step and that hornblende and clinozoisite dominated the later melting when the small mode of biotite was consumed. Biotite controls the Cu, Cs and, to a less extent, Rb and Ba concentrations in the host. Clinozoisite dominantly controls the concentrations of the REE, especially the LREE (Fig. 5). Hornblende in the dioritic gneiss displays a number of differences in trace element composition when compared with garnet in leucosomes and trondhjemitic veins (Fig. 4a,b,e). Garnet in the leucosomes, and trondhjemitic veins in either dioritic or gabbroic gneiss in the Pembroke Granulite has similar trace element patterns. Garnet from dioritic leucosomes displays only subtly lower Y and REE-values, and a tendency towards higher Li values. The similarity of trace element patterns in garnet from dioritic leucosomes and trondhjemitic veins in the Pembroke Granulite support the interpretation of Daczko *et al*. (2001a) that melting of the dioritic gneiss was the source of the trondhjemitic veins. The similarities of the trace element patterns in plagioclase from dioritic gneiss, its leucosomes and trondhjemitic veins that cut dioritic gneiss also reinforce a link between the dioritic gneiss as the source of the minerals in trondhjemitic veins (Fig. 4j,l).

Geochemistry of the GRZ

Previous studies (e.g. Clarke *et al*., 2000; Daczko *et al*., 2001a) have inferred that the GRZ, which mantle trondhjemitic veins in the gabbroic gneiss were formed through the divariant dehydration reaction (modelled in CNFMASH, Clarke *et al*., 2000):

$$\text{Paragasitic-hornblende} + \text{orthopyroxene} + \text{plagioclase} \rightarrow \text{garnet} + \text{clinopyroxene} + \text{quartz} + H_2O \quad (2)$$

Whole rock major and trace element analysis of adjacent samples of gabbroic gneiss and GRZ suggest that this reaction was essentially isochemical (Oliver, 1977; Blattner & Black, 1980; Bradshaw, 1989; Turner, 1998; Daczko *et al*., 2001a), with the exceptions of water loss, presumably to the melt, the depletion of Na and enrichment of Cu in the GRZ (Papadakis, 2000; Stevenson, 2000; Daczko *et al*., 2001a).

Figure 6 presents a cartoon illustrating the distribution of trace elements in the gabbroic gneiss, based on the ICPMS-data and modes of the reactants involved in reaction 2. The figure reflects the dominance of hornblende on the trace element budget in the gabbroic gneiss. Garnet formed in the GRZ mimics the hornblende pattern, in particular, that of the REE (Fig. 4c,d). Furthermore, clinopyroxene in both gabbroic gneiss and the GRZ display nearly identical trace element patterns. Data for rock samples from elsewhere (e.g. Witt-Eickschen & Harte, 1994) display the capability of clinopyroxene to vary in trace element composition by up to two orders of magnitude. On the other hand, only subtly greater enrichment was observed for B in plagioclase from the GRZ when

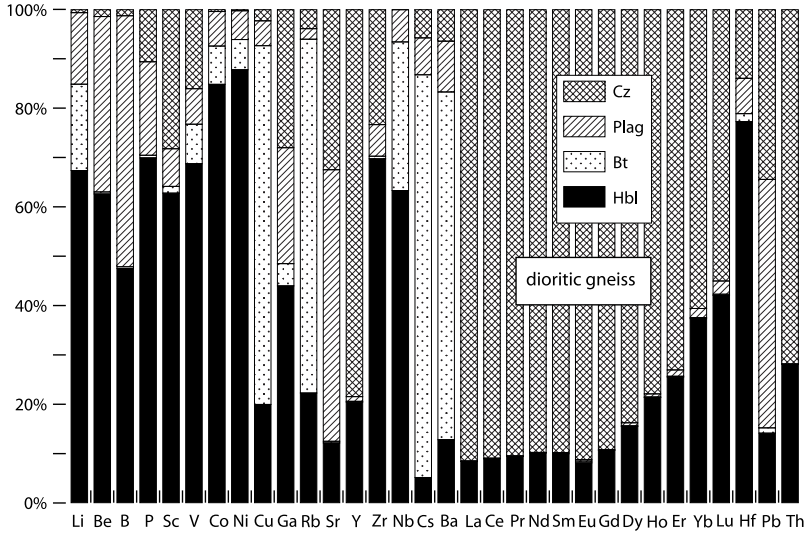

Fig. 5. Column-graph illustrating the trace-element budget for the major minerals present in dioritic gneiss that participate as reactants in reaction 1. The results of laser-ablation analyses of these minerals were averaged and multiplied by representative modal data collected by point counting sample 9805 ($n = 500$ with plagioclase: 45.2%; hornblende: 36.1%; clinozoisite: 9.5% and biotite: 2.5%).

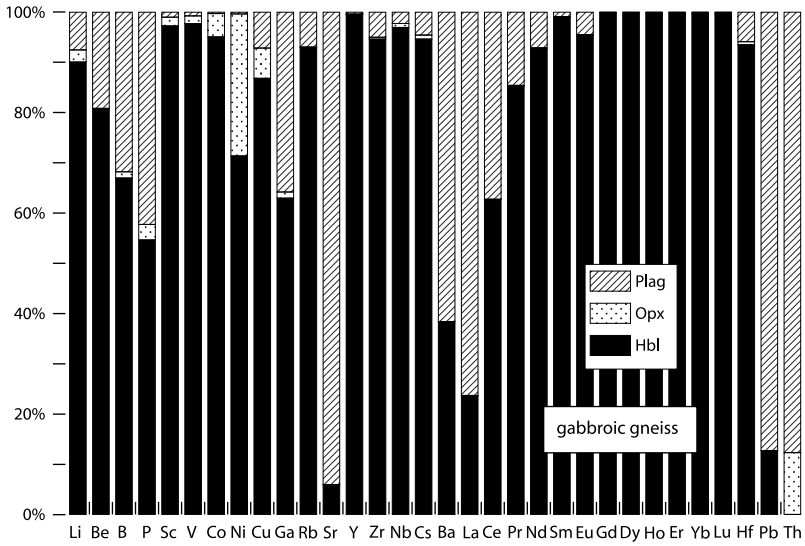

Fig. 6. Column-graph illustrating the trace-element budget for the major minerals in the gabbroic gneiss that participate as reactants in reaction 2. The results of laser-ablation analyses of these minerals were averaged and multiplied by representative modal data collected by point counting sample PK28 ($n = 500$ with plagioclase: 53.5%; hornblende: 38.7% and orthopyroxene: 2.0%).

compared with plagioclase from the gabbroic gneiss, while Ba is slightly less enriched.

The ICPMS-analyses presented in this paper demonstrate that the transformation of gabbroic gneiss (hornblende granulite) to the GRZ (garnet granulite) involved only minor redistribution of trace elements between reactant and product minerals. This is best displayed by the trace element pattern of garnet inherited from hornblende.

As described above, the trace element patterns within the gabbroic and dioritic gneiss samples from the Pembroke Granulite reveal consistent, distinct trace element patterns for garnet within the trondhjemitic veins/dioritic gneiss leucosomes, and GRZ. Gabbroic gneiss sample PK28 from Lake Pukutahi (*c*. 5 km NE of the Pembroke Granulite) has garnet in a trondhjemitic vein and adjacent GRZ with similar trace element patterns to each other and Pembroke Granulite GRZ garnet. No dioritic gneiss that could represent a local melt source was observed within low-strain zones at Lake Pukutahi. We therefore infer that the source rock for the Lake Pukutahi trondhjemitic veins is different to that observed in the dioritic gneiss of the Pembroke Granulite. Furthermore, the source of the trondhjemitic veins at Lake Pukutahi most likely contained similar gross trace-element patterns to the gabbroic gneiss of the Pembroke Granulite and Lake Pukutahi areas.

Distribution of trace elements during partial melting of mafic crust

The trace element content of any magma is controlled by the reactants involved in the melting, and any subsequent modification. The migmatitic textures preserved in dioritic gneiss of the Pembroke Granulite indicate that hornblende and clinozoisite, with or without biotite, controlled the trace element budget of the main peritectic phases and melt products. However, Daczko *et al.* (2001a) showed that the migrating magma interacted extensively with the host gabbroic gneisses to form the GRZ. Their whole-rock geochemical data indicate that the migrating silicate liquid gained water and Na_2O, leaving behind cumulate material to form the trondhjemitic veins. Although the trace element pattern of magma escaping from Pembroke Granulite was presumably mostly controlled by the initial partial melting step in the dioritic gneiss, interaction with sub-solidus gabbroic rocks would have modified these patterns very early in the ascent path.

CONCLUSIONS

The *in-situ* analysis of mineral trace element patterns provides a powerful means of characterizing patterns inherited by peritectic products during partial melting, and back-tracing mobilisate to a source. Distinctive trace element patterns in garnet from high-*P* mafic granulites in northern Fiordland demonstrate a link between migmatitic textures in dioritic gneiss and garnet-bearing trondhjemitic leucosomes that invade adjacent gabbroic gneiss. Trace element signatures preserved in the peritectic garnet are consistent with incongruent partial melting having been mostly controlled by the breakdown of hornblende and clinozoisite, garnet having inherited trace elements from both of these reactants. Accumulated melt propagated via fissures that were either already present or induced by a positive volume change related to the melting step. The hydrophilic nature of the mobilisate led to dehydration of the gabbroic gneiss adjacent to the fractures, water being released from hornblende breakdown to form the GRZ. Garnet in the GRZ inherited a trace element signature from S1 hornblende in the gabbroic gneiss that is distinct from that of garnet in the trondhjemitic veins and migmatitic textures of the dioritic gneiss.

ACKNOWLEDGEMENTS

Funding to support this work was provided by a large Australian Research Council grant to G.L. Clarke and K.A. Klepeis (DP0342862). An International Postgraduate Award supported FCS, and Australian Postgraduate Awards supported JAS and NRD. We are especially grateful to A. Sharma and S. Elhlou for their instruction and assistance with the LA-ICPMS. We thank R.L. Turner and A. Papadakis for their enthusiastic assistance in the field, and T. Rushmer for discussions. We are grateful to the Department of Conservation in Te Anau for permission to visit and sample localities in Fiordland National Park. This is publication no. 328 in ARC National Key Centre for Geochemical Evolution and Metallogeny of Continents (http://www.es.mq.edu.au/GEMOC).

REFERENCES

Antignano, A. IV, Rushmer, T., Daczko, N. R., Clarke, G. L., Collins, W. J. & Klepeis, K. A., 2001. Partial melting of a hornblende–biotite–clinozoisite-bearing metadiorite: applications to the deep crust, Fiordland, New Zealand. *Geological Society of America*, **33,** 6, 211 (Abstracts with Programs).

Atherton, M. P. & Petford, N., 1993. Generation of sodium-rich magmas from newly underplated basaltic crust. *Nature*, **362,** 144–146.

Bea, F., Pereira, M. D. & Stroh, A., 1994. Mineral/leucosome trace-element partitioning in a peraluminous migmatite (a laser ablation-IC-PMS study). *Chemical Geology*, **117,** 291–312.

Blattner, P., 1976. Replacement of Hornblende by Garnet in Granulite Facies Assemblages near Milford Sound, New Zealand. *Contributions to Mineralogy and Petrology*, **55,** 181–190.

Blattner, P., 1991. The North Fiordland transcurrent convergence. *New Zealand Journal of Geology and Geophysics*, **34,** 533–542.

Blattner, P. & Black, P. M., 1980. Apatite and Scapolite as Petrogenetic indicators in Granolites of Milford Sound, New Zealand. *Contributions to Mineralogy and Petrology*, **74,** 339–348.

Bradshaw, J. Y., 1989. Early Cretaceous vein-related garnet granulite in Fiordland, southwest New Zealand: a case for infiltration of mantle-derived CO_2-rich fluids. *Journal of Geology*, **97,** 697–717.

Clarke, G. L., Klepeis, K. A. & Daczko, N. R., 2000. Cretaceous high-*P* granulite at Milford Sound, New Zealand: their metamorphic history and emplacement in a convergent margin setting. *Journal of Metamorphic Geology*, **18,** 359–374.

Daczko, N. R., Clarke, G. L. & Klepeis, K. A., 2001a. Transformation of two-pyroxene hornblende granulite to garnet granulite involving simultaneous melting and fracturing of the lower crust, Fiordland, New Zealand. *Journal of Metamorphic Geology*, **19,** 547–560.

Daczko, N. R., Klepeis, K. A. & Clarke, G. L., 2001b. Evidence of Early Cretaceous collisional-style orogenesis in northern Fiordland, New Zealand and its effects on the evolution of the lower crust. *Journal of Structural Geology*, **23,** 693–713.

Daczko, N. R., Stevenson, J. A., Clarke, G. L. & Klepeis, K. A., 2002. Successive hydration and dehydration of a high-*P* mafic granofels involving clinopyroxene-kyanite symplectites, Mt Daniel, Fiordland, New Zealand. *Journal of Metamorphic Geology*, **20,** 669–682.

Defant, M. J. & Drummond, M. S., 1990. Derivation of some modern arc magmas by melting of young subducted lithosphere. *Nature*, **347,** 662–665.

Hill, E. J., 1995. A deep crustal shear zone exposed in western Fiordland, New Zealand. *Tectonics*, **14,** 1172–1181.

Hollis, J. A., Clarke, G. L., Klepeis, K. A., Daczko, N. R. & Ireland, T. R., 2003. Geochronology and geochemistry of high-pressure granulites of the Arthur River Complex, Fiordland, New Zealand: Cretaceous magmatism and metamorphism on the Palaeo-Pacific Margin. *Journal of Metamorphic Geology*, **21,** 299–313.

Norman, M. D., Pearson, N. J., Sharma, A. & Griffin, W. L., 1996. Quantitative analysis of trace elements in geological materials by laser ablation ICPMS: instrumental operating conditions and calibration values of NIST glasses. *Geostandards Newsletter*, **20,** 247–261.

Norman, M. D., Griffin, W. L., Pearson, N. J., Garcia, M. O. & O'Reilly, S. Y., 1998. Quantitative analysis of trace element abundances in glasses and minerals: a comparison of laser ablation ICPMS, solution ICPMS, proton microprobe, and electron microprobe data. *Journal of Analytical Atomic Spectroscopy*, **13,** 477–482.

Oliver, G. J. H., 1977. Feldspathic hornblende and garnet granulites and associated anorthosite pegmatites from Doubtful Sound, Fiordland, New Zealand. *Contributions to Mineralogy and Petrology*, **65,** 111–121.

Papadakis, A., 2000. High pressure partial melting of the lower crust: constraints from the Pembroke Granulite and Milford Gneiss, Fiordland, New Zealand. Unpublished BSc (Honours) Thesis, The University of Sydney, Sydney.

Stevenson, J. A., 2000. Emplacement and post-intrusional history of a Cretaceous batholith: evidence from the contact between the Western Fiordland Orthogneiss and the Arthur River Complex, at Mt Daniel, Fiordland, New Zealand. Unpublished BSc (Honours) Thesis, The University of Sydney, Sydney.

Taylor, S. R. & McLennan, S. M., 1985. *The Continental Crust: Its Composition and Evolution*. Blackwell, Oxford, 312 pp.

Tulloch, A. J., Ireland, T. R., Walker, N. W. & Kimbrough, D. L., 2000. U–Pb zircon ages from the Milford Orthogneiss, Milford Sound, northern Fiordland: Paleozoic igneous emplacement and Early Cretaceous metamorphism. *Institute of Geological & Nuclear Sciences Science Report*, **6,** 14.

Turner, R. L., 1998. Strain patterns and recrystallization in the lower crust; evidence from Garnet Reaction Zones Fiordland, New Zealand. Unpublished BSc (Hons) Thesis, The University of Sydney, Sydney.

Witt-Eickschen, G. & Harte, B., 1994. Distribution of trace elements between amphibole and clinopyroxene from mantle peridotites of the Eifel (western Germany): an ion-microprobe study. *Chemical Geology*, **117,** 235–250.

Yamamoto, H. & Yoshino, T., 1998. Superposition of replacements in the mafic granulites of the Jigal complex of the Kohistan arc, northern Pakistan: dehydration and rehydration within deep arc crust. *Lithos*, **43,** 219–234.

Received 3 February 2003; revision accepted 20 March 2004.